81-DET-47

THE AMERICAN SOCIETY OF MECHANICAL ENGINEERS
345 E 47 St., New York, N.Y. 10017

Comparison of the Unbalance Responses of Jeffcott Rotors With Shaft Bow and Shaft Runout

R. D. Flack
Associate Professor,
Mem. ASME

J. H. Rooke
Research Associate,
Mem. ASME

J. R. Bielk
Research Associate,
Mem ASME

E. J. Gunter
Professor,
Mem. ASME

Department of Mechanical and Aerospace Engineering,
School of Engineering and Applied Science,
University of Virginia,
Charlottesville, Va. 22901

The unbalance response of a Jeffcott rotor with shaft bow and/or runout was theoretically and experimentally studied. Bow refers to a rotor which is warped; bow is a function of running speed. Runout refers to electrical or mechanical asymmetrics of the shaft and is not dynamical. Included in the theoretical model is the capability of low-speed response compensation, such that the response at low speed can be vectorially subtracted from the total response at any rotational speed. Responses of rotors with equal amounts of bow or runout are shown to be significantly different in both Bode and Nyquist forms. Using low speed compensation is shown to "correct" the unbalance response of a rotor with runout to an ideal (unbowed - no runout) case. The amplitude response plot of a bowed rotor is not corrected to the ideal response plot by the use of such compensation; however, the shape of the phase response plot closely resembles the ideal case for most cases. A small scale lightly damped Jeffcott rotor rig was also tested. The magnitude and angular position of the shaft bow were parametrically varied. The vibration data from the rotor tests were plotted using a synchronous tracking filter by two methods: both not using and using low speed compensation. Experimental data agree excellently with predictions for a bowed rotor for all cases and differences less than 8 percent were usually found.

Introduction

Knowledge of the synchronous amplitude and phase angle and total amplitude of vibration is of utmost importance in balancing and understanding most rotor applications. Inductance or eddy current probes are one of the most common instruments used to detect shaft vibration in rotating machinery. Rotor bow and shaft runout are two phenomena that affect the observed response of a rotor. In this paper, differences in the responses due to these two phenomena are identified, and methods of experimental "runout compensation" are studied. Both theoretical predictions and experimental data are presented.

Displacement probes and the related processing equipment are used for three basic purposes. First, when a system is running on line (such as a power generating unit), vibration monitors are needed as safety devices, such that if the rotor vibratory amplitude grows, alarm and danger warnings can be initiated, and, under many conditions, the system will be automatically shut down [1]. Second, by measuring the vibrational response of the rotor at various speeds, one can determine the angular location and magnitude of a rotor unbalance, such that the system can be balanced [2,3]. Third, by analyzing the vibration response as a function of rotor speed, one can determine important system parameters, such as amplification factor or damping [4], which are independent of rotor unbalance.

The simplest rotor that can be studied is one with a perfectly straight, round, and angularly uniform material shaft. Unfortunately, such a rotor rarely exists in practice. Any shaft material nonuniformities modify the observed motion of the shaft due to the inductance principles of the probes. For example, at very low speeds where no vibrations exist, a probe will measure apparent shaft motion due to this effect. This effect is termed electrical runout and is not a function of shaft rotational speed. A second similar effect is due to out-of-roundness or scratches on the surface of the shaft. This is termed mechanical runout and also is not a function of shaft speed.

The third deviation from an ideal rotor is due to a bowed or warped shaft. Several applications in which shaft bow is important in the balancing of the rotor are gas turbines, nuclear reactor water pumps, steam turbines, and the space shuttle main engine. Such bow can result from an extended gravity sag, thermal distortion, a large previous unbalance, or a variety of other reasons, and the bow is a function of shaft speed.

Previous to this time, several authors have theoretically examined and discussed the problem of a warped shaft [5-9]. Nicholas, et al. [5], indicate that the rotor bow can significantly affect the Bode response of a rotor, and the effect is a function of rotational speed.

Some studies have also been presented in which a rotor with a bowed shaft was balanced experimentally [10,11]. However,

Contributed by the Vibration and Sound Committee for presentation at the Design Engineering Technical Conference, Hartford, Conn., Sept. 20-23, 1981 of THE AMERICAN SOCIETY OF MECHANICAL ENGINEERS. Manuscript received at ASME Headquarters June 4, 1981. Paper No. 81-DET-47.
Copies will be available until June 1982.

experimental results have not yet been presented in the open literature in which the behavior of a bowed rotor is studied. The theoretical results in reference [5] have not been verified by an experimental program.

In practice, one can observe a shaft vibration at low speeds. In many cases, one cannot distinguish the contributions from the three nonideal effects previously described. For example, a probe may be located "deeply" in a machine, such that using a dial indicator to determine the mechanical runout at the probe location may not be possible. The resultant measured vibration vector is a sum of the three vectors from electrical runout, mechanical runout, and shaft bow. An instrument which is used to cancel the first two nonideal contributions, is termed a "runout subtractor." This instrument subtracts a constant vibration vector from the monitored shaft vibration at all speeds. The constant vector is defined as the vibration vector measured at low speeds, where low means at speeds sufficiently low that dynamic effects are negligible. Unfortunately, since all three contributions are one sum, a runout subtractor compensates correctly for the first two, but introduces an error by subtracting a constant vector for the rotor bow. The response of a rotor to shaft bow is a function of speed. At low speed, the response is equal to shaft bow. However, at a rotor critical speed, the response to bow can be more than ten times the bow itself, and at high speeds, the response is nil regardless of bow [5]. Thus, by subtracting a constant vector, an error in the measured response is induced, particularly near the critical speed and at higher speeds.

The intentions of this paper are threefold: (1) to identify the differences between the observed vibratory responses of bowed rotors and the observed vibratory response of rotors that have either mechanical or electrical runout, (2) to identify problems associated with using runout subtractors with bowed rotors and to estimate the inaccuracies, and (3) to present experimental data verifying the predicted response of a bowed rotor [5]. A Jeffcott rotor is both modeled theoretically and tested experimentally.

Theoretical Model of Rotor

The equations of motion of a bowed rotor have been previously derived [5]. In this section, the model for runout and runout subtraction will be described.

In Fig. 1, a basic Jeffcott rotor with a bowed shaft and with an unbalance is presented. All phase angles are measured with

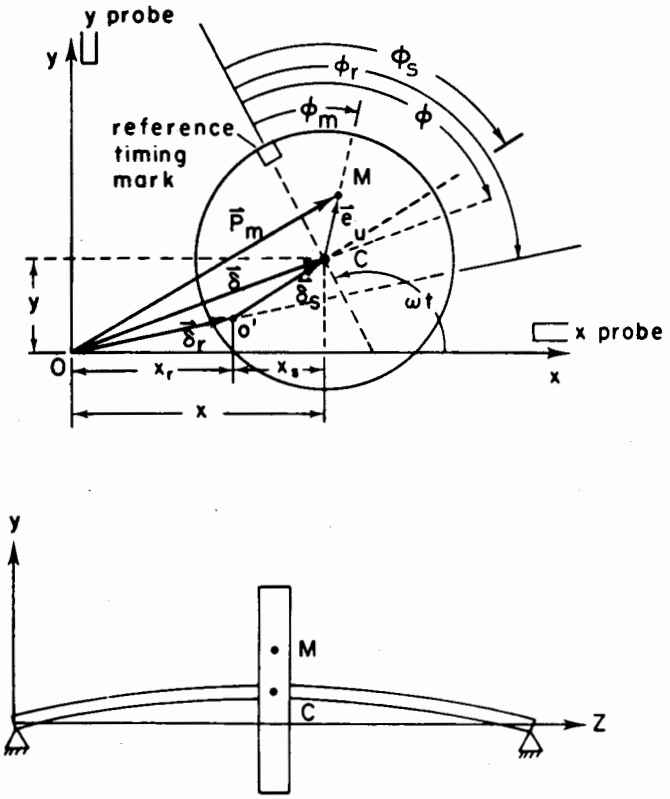

Fig. 1 Single mass flexible rotor with bowed shaft, end and side views

respect to a reference timing mark on the shaft. The shaft has a residual bow of magnitude δ_r and phase angle ϕ_r. The mass center of the disk is displaced a distance e_u from the shaft centerline which results in a dynamic response as the shaft rotates. The magnitude and phase angle of the dynamical response are δ_s and ϕ_s, respectively. The magnitude and phase angle of the combined electrical and mechanical runout are δ_o and ϕ_o, respectively. Thus, the total observed response is

$$\delta = \delta_r + \delta_s + \delta_o \tag{1}$$

No gyroscopics occur since the disk always rotates in its own plane. The shaft mass is considered negligible compared to the

Nomenclature

A = amplification factor, δ/e_u
c = shaft damping
c_{cr} = critical shaft damping, $2m\omega_{cr}$
$\mathbf{e}_u$ = unbalance eccentricity vector
f = frequency ratio, ω/ω_{cr}
k = shaft spring rate
m = disk mass
x = horizontal shaft centerline displacement
y = vertical shaft centerline displacement
z = complex shaft centerline displacement, $x + iy$
α_m = influence coefficient due to mass unbalance, $f^2/(1 - f^2 + 2i\zeta f)$
α_o = influence coefficient due to runout = 1
α_r = influence coefficient due to bow, $1/(1 - f^2 + 2i\zeta f)$
α_{rc} = influence coefficient due to compensated bow, $(f^2 - 2i\zeta f)/(1 - f^2 + 2i\zeta f)$
γ = angle between the bow vector and the mass unbalance vector
δ = total response vector at the center of the shaft
δ_o = runout vector
δ_r = bow vector
δ_s = response to the mass unbalance vector and the bow vector
ζ = damping ratio, c/c_{cr}
ζ_m = predicted measured damping ratio
ϕ = phase angle between the shaft centerline response vector and the timing mark
ϕ_m = angle between the mass unbalance vector and the timing mark
ϕ_o = angle between the rotor runout vector and the timing mark
ϕ_r = angle between the bow vector and the timing mark
ϕ_s = angle between the rotor response to mass unbalance vector and the timing mark
ω = rotational speed
ω_{cr} = rotor critical speed, $\sqrt{k/m}$

Subscripts

c = with low speed compensation
ce = compensation error term
cr = critical speed
0 = evaluated at $f = 0$

Superscripts

$-$ = nondimensionalized by e_u

rigid disk mass, and both the shaft and disk rotate with constant angular velocity, ω. The supports are taken as rigid.

Using the equation of motion for the simple rotor with mass unbalance and shaft bow, Nicholas, et al. [5], obtained the following steady state nondimensionalized rotor response as a function of rotor speed.

$$\bar{z}=\frac{\bar{\delta}_r e^{-i\phi_r}+f^2 e^{-i\phi_m}}{1-f^2+2i\zeta f} \tag{2}$$

where all of the parameters are defined in the Nomenclature.

Consider a shaft with electrical and/or mechanical runout. This runout is represented as a vector, δ_o, at a phase angle of ϕ_o. The runout vector is also nondimensionalized by the unbalance eccentricity ($\bar{\delta}_o = \delta_o/e_u$). As was mentioned earlier, this runout vector is constant and independent of shaft rotational speed. Using the principle of superposition, this constant response due to runout may be added to equation (2) for steady state response yielding

$$\bar{z}=\frac{\bar{\delta}_r e^{-i\phi_r}+f^2 e^{-i\phi_m}}{1-f^2+2i\zeta f}+\bar{\delta}_o e^{-i\phi_o} \tag{3}$$

For convenience, let $\gamma = \phi_r - \phi_m$. Next, equation (3) can be put in the form:

$$\bar{z}=\alpha_r\bar{\delta}_r e^{-i\phi_r}+\alpha_m e^{-i\phi_m}+\alpha_o\bar{\delta}_o e^{-i\phi_o} \tag{4}$$

where α_r, α_m, and α_o are the influence coefficients for the bow, mass unbalance, and runout and are defined in the Nomenclature.

Separate $\bar{z}$ into real and imaginary components, $\bar{z} = \bar{z}_r + i\bar{z}_i$, to obtain

$$\bar{z}_r=\frac{(\bar{\delta}_r\cos\phi_r+f^2\cos\phi_m)(1-f^2)-2\zeta f(\bar{\delta}_r\sin\phi_r+f^2\sin\phi_m)}{(1-f^2)^2+(2\zeta f)^2}+\bar{\delta}_o\cos\phi_o \tag{5a}$$

$$\bar{z}_i=-\left[\frac{(\bar{\delta}_r\sin\phi_r+f^2\sin\phi_m)(1-f^2)+2\zeta f(\bar{\delta}_r\cos\phi_r+f^2\cos\phi_m)}{(1-f^2)^2+(2\zeta f)^2}+\bar{\delta}_o\sin\phi_o\right] \tag{5b}$$

The shaft amplification factor and phase angle are

$$A=\sqrt{\bar{z}_r^{\,2}+\bar{z}_i^{\,2}} \tag{6a}$$

and

$$\phi=\tan^{-1}[\bar{z}_i/\bar{z}_r] \tag{6b}$$

As was stated earlier, a runout subtractor or compensator measures the rotor "response" vector at slow roll, i.e., speeds sufficiently low such that shaft dynamics are not encountered, and subtracts this constant vector from the rotor response at all other speeds. Thus, for the case of an unbowed shaft, it compensates for shaft runout, thereby presenting the response for the rotor as if it had only unbalance with no runout. To understand what the output from a compensator represents for the observed response of a bowed rotor at slow roll, substitute $f = 0$ into equation (3)

$$\bar{z}_0=\bar{\delta}_r e^{-i\phi_r}+\bar{\delta}_o e^{-i\phi_o} \tag{7}$$

$$\bar{z}_r\Big|_0=\bar{\delta}_r\cos\phi_r+\bar{\delta}_o\cos\phi_o \tag{8a}$$

$$\bar{z}_i\Big|_0=-\bar{\delta}_r\sin\phi_r-\bar{\delta}_o\sin\phi_0 \tag{8b}$$

Equations (7) and (8) are the quantities the compensator subtracts from the total response at all other speeds. Define $\bar{z}_c$ as the total response of a bowed rotor compensated for electrical/mechanical runout

$$\bar{z}_c=\bar{z}-\bar{z}_0=\frac{\bar{\delta}_r e^{-i\phi_r}+f^2 e^{-i\phi_m}}{1-f^2+2i\zeta f}-\bar{\delta}_r e^{-i\phi_r} \tag{9}$$

Rearranging and combining like terms in equation (9) yields

$$\bar{z}_c=\frac{(f^2-2i\zeta f)\bar{\delta}_r e^{-i\phi_r}+f^2 e^{-i\phi_m}}{1-f^2+2i\zeta f} \tag{10}$$

which can be put in the form

$$\bar{z}_c=\alpha_{rc}\bar{\delta}_r e^{-i\phi_r}+\alpha_m e^{-i\phi_m} \tag{11}$$

where α_{rc} and α_m are influence coefficients for the compensated bow and mass unbalance. For large values of f, α_{rc} approaches α_m, indicating the responses due to a compensated blow and an equal unbalance eccentricity are equal.

Also, one can define $\bar{z}_r|_c$ and $\bar{z}_i|_c$ as the real and imaginary components, respectively, of the response of a bowed rotor with runout after compensation.

$$\bar{z}_r\Big|_c=\bar{z}_r-\bar{z}_r\Big|_0=$$

$$\frac{(\bar{\delta}_r\cos\phi_r+f^2\cos\phi_m)(1-f^2)-2\zeta f(\bar{\delta}_r\sin\phi_r+f^2\sin\phi_m)}{(1-f^2)^2+(2\zeta f)^2}$$
$$+\bar{\delta}_o\cos\phi_o-[\bar{\delta}_r\cos\phi_r+\bar{\delta}_o\cos\phi_o] \tag{12a}$$

$$\bar{z}_i\Big|_c=\bar{z}_i-\bar{z}_i\Big|_0=$$

$$-\left[\frac{(\bar{\delta}_r\sin\phi_r+f^2\sin\phi_m)(1-f^2)+2\zeta f(\bar{\delta}_r\cos\phi_r+f^2\cos\phi_m)}{(1-f^2)^2+(2\zeta f)^2}\right]$$
$$+\bar{\delta}_o\sin\phi_o-[-\bar{\delta}_r\sin\phi_r-\bar{\delta}_o\sin\phi_o] \tag{12b}$$

These values may now be substituted into equation (6) yielding A_c and ϕ_c, the response amplitude and phase after compensation. Upon inspection of the foregoing equations, one can see that an error is introduced. Since shaft runout is constant with speed, the subtraction of a constant runout vector correctly compensates for this effect (i.e., the shaft runout terms all cancel). However, since the response due to shaft bow is not constant with speed, the subtraction of the constant slow roll bow vector clearly does not adequately compensate for this effect. Shaft bow terms remain in the compensated rotor response equations. Carrying out the subtraction in equation (12), the bow response terms that remain may be called compensation error terms.

$$\bar{z}_r\Big|_{ce}=\bar{\delta}_r\cos\phi_r\left[\frac{1-f^2}{(1-f^2)^2+(2\zeta f)^2}-1\right]$$
$$-\frac{2\zeta f\bar{\delta}_r\sin\phi_r}{(1-f^2)^2+(2\zeta f)^2} \tag{13a}$$

$$\bar{z}_i\Big|_{ce}=-\bar{\delta}_r\sin\phi_r\left[\frac{1-f^2}{(1-f^2)^2+(2\zeta f)^2}-1\right]$$
$$-\frac{2\zeta f\bar{\delta}_r\cos\phi_r}{(1-f^2)+(2\zeta f)^2} \tag{13b}$$

Note that for low speeds ($f \cong 0$), these error terms are negligible but become quite pronounced at speeds approaching the critical speed and higher. Thus, the response of a bowed rotor with compensation does not represent the response of a rotor with unbalance only. In the next section, similarities and differences will be demonstrated.

For the foregoing equations, the response was found for any value of ϕ_m. For the remainder of this paper, the unbalance vector, $\mathbf{e}_u$, has been assumed to be in line with the

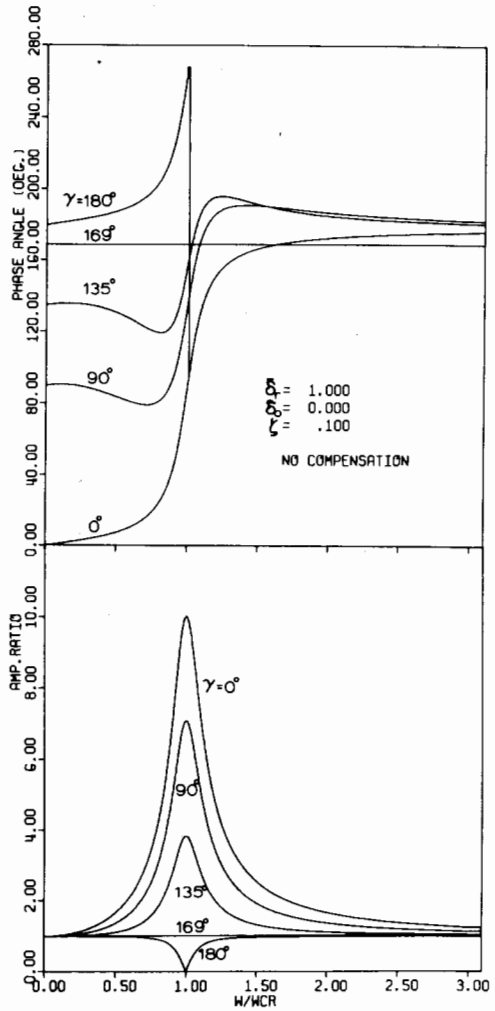

Fig. 2 Response curve without compensation with $\zeta = 0.1$ and $\delta_r = 1.00$ for various γ values

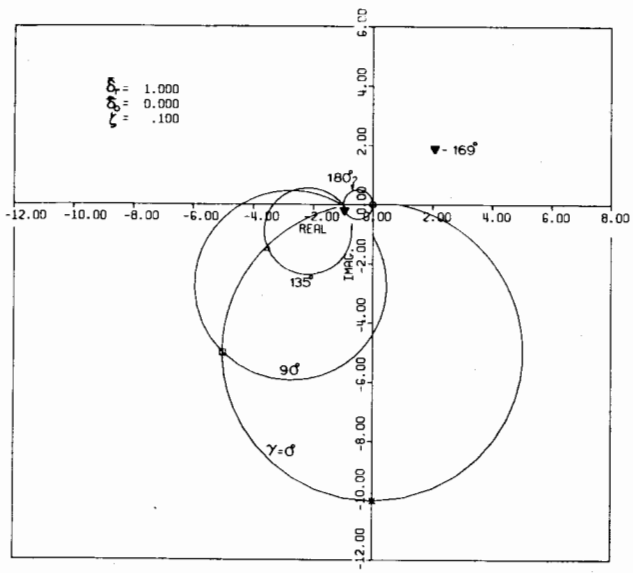

Fig. 3 Nyquist response curves for $\zeta = 0.1$ and $\delta_r = 1.00$

reference timing mark, so that $\phi_m = 0$. This latter assumption does not reduce the generality of the solution, since the timing mark is an arbitrary reference point. For example, the actual amplitude of response will not depend on the reference mark location. Also, since $\gamma = \phi_r - \phi_m$, the angle, γ, will be equal to ϕ_r if $\phi_m = 0$.

Theoretical Results

In the previous section, a model for runout compensation was developed. In this section, typical parametric studies are presented. Synchronous response plots (hereafter called Bode) and complex response plots (hereafter called Nyquist) from both a bowed rotor and a rotor with runout are presented and differences are discussed. Also, responses with runout compensation are presented and discussed.

In Fig. 2, Bode response plots are shown for a bowed rotor ($\bar{\delta}_r = 1.00$) with low damping ($\zeta = 0.1$) and no runout. Results for five values of γ are presented. In Fig. 3, Nyquist forms of the previous plots are shown. Finally, Bode response plots with constant compensation are presented in Fig. 4.

In Figs. 5-7, response plots for a rotor with only runout ($\bar{\delta}_o = 1.00$ and $\zeta = 0.10$) are shown in the same fashion as the bowed rotor responses (Figs. 2-4) for four values of ϕ_o. Thus, the low speed response of this rotor without compensation is identical to that presented in Figs. 2-4.

By comparison of Figs. 2 and 5, one can see several differences in the Bode responses of a bowed rotor and a rotor with runout with equal low speed responses. For example, the maximum amplitude of a bowed rotor is strongly dependent on γ while the maximum response for a rotor with runout is weakly dependent on ϕ_o. The minimum amplitude for a bowed rotor is zero ($\gamma = 180$ deg) and occurs at $\omega/\omega_{cr} = 1.00$, while the minimum nondimensionalized amplitude for a rotor with runout is 0.28 ($\phi_o = 180$ deg) and occurs at $\omega/\omega_{cr} = 0.7$.

The phase angle responses are also different for the rotors (Figs. 2 and 5). For $\gamma = 0$ deg and $\phi_o = 0$ deg, the responses are similar. However, for γ and $\phi_o = 90$ deg and 135 deg, the shapes of the responses are different, particularly at low speeds. For γ and $\phi_o = 180$ deg, significant differences are observed. Particularly at $\omega/\omega_{cr} = 1$, a sudden shift of 180 deg is shown for the bowed rotor, but no such sudden shift is observed for a rotor with runout.

The differences can be seen also by Nyquist plots (Figs. 3 and 6). For the bowed rotor (Fig. 3), the response is nearly circular as is the response for a simple straight shaft in a lightly damped system. However, the sizes of the response circles depend strongly on the value of γ. The responses at the critical speeds are marked with symbols. The maximum response is for 0 deg, while the minimum response is for 180 deg. On the other hand, since the response of a rotor with only runout is simply the response due to unbalance plus a constant vector, the sizes of the response circles in Fig. 6 are not a function of ϕ_o.

The effect of constant compensation is to shift the low speed response for each of the circles to the origin. For the cases in Fig. 6, all four circles collapse to one circle. However, for Fig. 3, five separate response circles remain because they are of different radii. By examining the compensated Bode plots for the rotor with runout (Fig. 7), one can see that all of the phase and amplitude responses are identical to a simple rotor (no bow, no runout) with unbalance ($\zeta = 0.1$). This is termed the "ideal" case.

Three occurrences can be observed from the Nyquist plots.

(*a*) The responses were all circular in shape. No "minor" or "inside loops" were observed. These secondary loops occur as a result of disk skew [12] or foundation resonances [13], but never as a result of bow or runout alone.

(*b*) Note that the Nyquist "circle" for the case of $\bar{\delta}_r = 1.0$, $\gamma = 0$ deg (Fig. 3) closely approximates the locus of points representing the critical speed responses for all values of γ. Substituting $f = 1$ and $\bar{\delta}_o = 0$ into equation (5) and manipulating yields

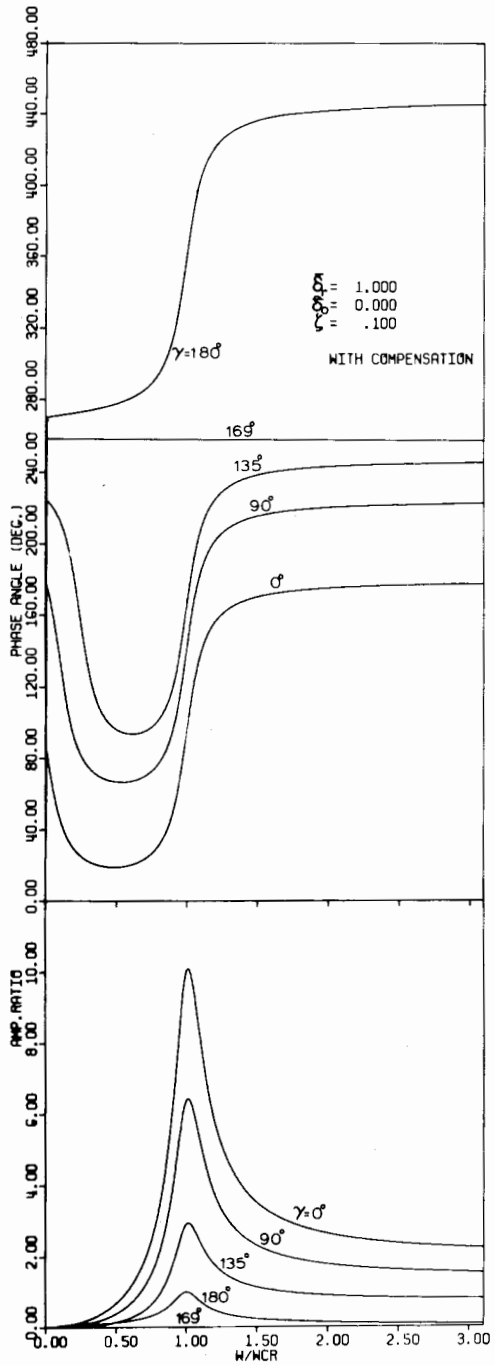

Fig. 4 Response curves with compensation for $\zeta = 0.1$ and $\bar{\delta}_r = 1.00$ for various γ values

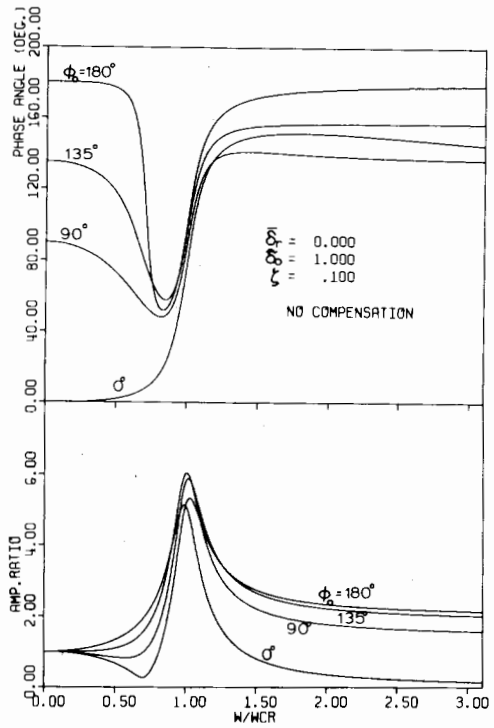

Fig. 5 Response curves without compensation for $\zeta = 0.1$ and $\bar{\delta}_o = 1.00$ for various ϕ_o values

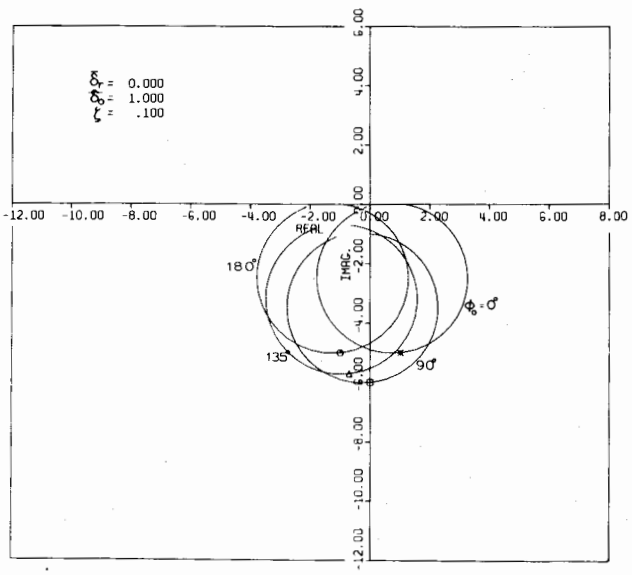

Fig. 6 Nyquist response curves for $\zeta = 0.1$ and $\bar{\delta}_o = 1.00$

$$\bar{z}_r{}^2{}_{cr} + (\bar{z}_{i_{cr}} + 1/2\zeta)^2 = (\bar{\delta}_r/2\zeta)^2 \quad (14)$$

This is the general locus of points of the critical speed response for a given value of ζ. Thus, the center is at the point $(0, -1/2\zeta)$ and the radius is $(\bar{\delta}_r/2\zeta)$. One should note that if shaft runout is also present, the radius of the critical speed response circle will be unchanged, but the center will be displaced by an amount equal to the shaft runout vector.

(*c*) For a bowed rotor with $\bar{\delta}_r = 1.00$ and for cases of γ slightly less than 180 deg (say $\gamma = 169$ deg), the net phase shift as a rotor traverses a critical speed is approximately zero when compensation is not used. However, if γ is slightly greater than 180 deg (say 190 deg, not shown for the sake of clarity), the Nyquist loop encircles the origin which results in a phase shift of approximately 360 deg. Such behavior has been reported for a large scale test rig [14]. This is particularly important since most rotors are balanced at the critical speed, i.e., ideally $\bar{\delta}_r = 1.00$ and $\gamma = 180$ deg [5]. However, practical limitations usually cause both $\bar{\delta}_r$ and γ to be slightly different from the ideal balance resulting in net 0 deg or 360 deg phase shifts in practice.

In Fig. 4, results are presented for the response of a bowed rotor with runout compensation applied. Results in Fig. 7 represent the response of an ideal rotor. Thus, by comparing Figs. 4 and 7, several errors can be seen (which are also predicted by equation (13)).

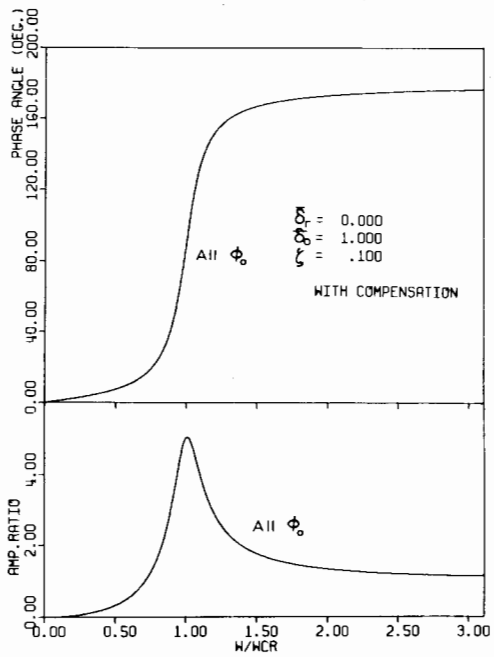

Fig. 7 Response curves with compensation for $\zeta = 0.1$ and $\bar{\delta}_o = 1.00$ for various ϕ_o values (ideal response)

(a) At high speeds, the compensated amplitude response does not approach the unbalance eccentricity ($\bar{z} = 1.00$); for large values of $\bar{\delta}_r$ (i.e., small values of e_u), the "observed" amplitude response at high speed approaches $\bar{\delta}_r$. The bowed rotor response with no compensation does approach unity, however.

(b) The maximum amplitude response remains a strong function of γ.

(c) The actual values of phase angle are approximately correct only for $\gamma = 0$ deg and ω/ω_{cr} greater than 0.7.

(d) The shapes of the phase angle curves are completely incorrect for values of ω/ω_{cr} less than 0.7 for all values of γ except 180 deg.

Of particular interest are the shapes of the phase angle curves for the compensated bowed rotor (Fig. 4). For all values of γ shown, the shapes of the phase angle curves for ω/ω_{cr} greater than 0.7 in general closely resemble the ideal phase angle curve. For example, if one has a phase angle response plot, a typical method of "measuring" a system damping is by the following, which is valid for a rotor without bow or runout.

$$\zeta_m = 180/[\pi\omega_{cr}(d\phi/d\omega)]_{\omega=\omega_{cr}} \tag{15}$$

One can evaluate $d\phi/d\omega$ for the present method by two techniques: (a) measuring the slope of ϕ versus ω/ω_{cr} as in Fig. 4, or (b) by differentiating equation (6b) and subsequently equation (12) for a compensated rotor, or equation (5) for an uncompensated rotor. The latter method was used, and the values of ζ_m which were obtained for $\zeta = 0.1$, $\bar{\delta}_r = 1.00$, $\bar{\delta}_o = 0.00$, and $\gamma = 0$, 90, 135, 169, and 180 deg are presented in Table 1. Values of ζ_m were determined for cases with and without constant compensation. In Table 1, one can see that the measured values of ζ are very close to the actual value of ζ (0.100) for the compensated responses. However, the measured values of ζ are sometimes significantly different from the true value of ζ for the responses with no compensation. This is most easily understood by accurately examining the slopes on the ϕ versus ω/ω_{cr} plot in Fig. 2. At $\omega/\omega_{cr} = 1.00$, the slope for $\gamma = 135$ deg is less than that for $\gamma = 0$ deg, for example, yielding a larger measured value of damping.

Table 1 Values of ζ_m determined from Bode diagrams; ($\zeta = 0.1$, $\bar{\delta}_r = 1.00$, $\bar{\delta}_o = 0.00$)

γ	No compensation	With compensation
0 deg	0.100	0.101
90 deg	0.111	0.101
135 deg	0.132	0.102
169 deg	∞	∞
180 deg	0.100*	0.100

*indeterminate at $\gamma = 180$ deg, $\omega/\omega_{cr} = 1.00$; evaluated at $\gamma = 180$ deg, $\omega/\omega_{cr} = 1.01$

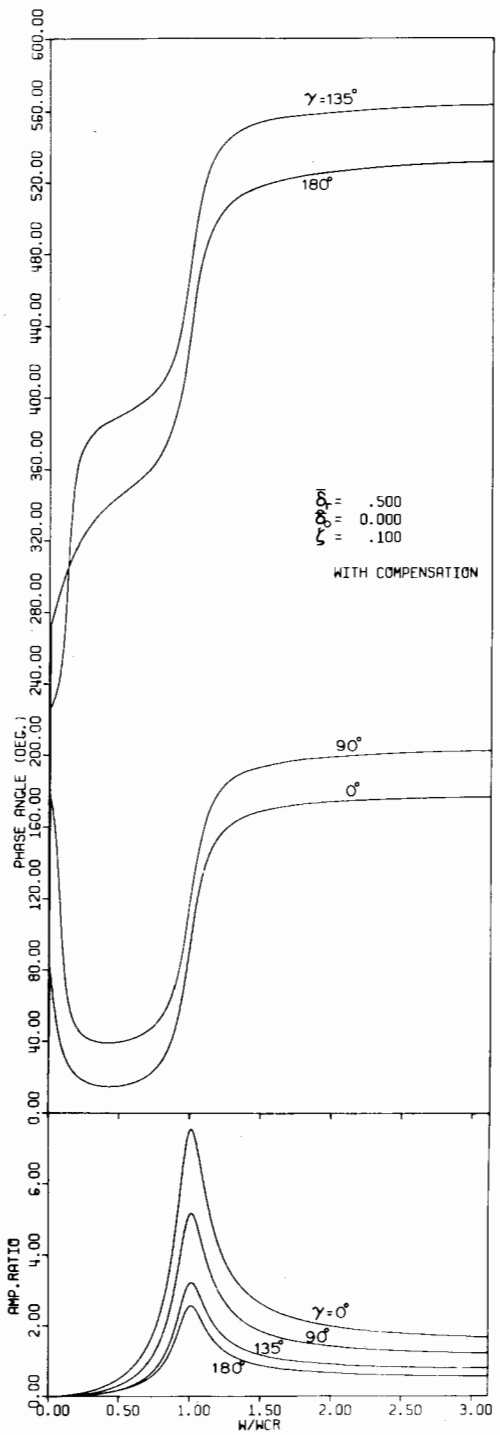

Fig. 8 Response curves with compensation for $\zeta = 0.1$ and $\bar{\delta}_r = 0.5$ for various γ values

One peculiarity of bowed rotor systems with $\bar{\delta}_r = 1.00$ is shown in Figs. 2-4. Namely, for $\gamma \simeq 169$ deg, the amplitude and phase responses are nearly constant with speed as shown in Fig. 2. In Fig. 3, the response is a short line. Likewise, the compensated response plots (Fig. 4) are approximately constant with speed resulting in $(d\phi/d\omega)_{\omega=\omega_{cr}} \simeq 0$. Thus, for this value of γ almost infinite damping is measured. One should realize that as ζ varies, the value of γ for which A and ϕ are constants also varies. When $\bar{\delta}_r = 1.00$, $\bar{z} = 1.00$ and $f = 1$, one can show, by solving the real part of equation (3), that this value of γ is given by

$$\gamma = \sin^{-1}(2\xi) \tag{16}$$

For comparison, a second case is shown for a bowed rotor with compensation. This is presented in Fig. 8 and is for $\bar{\delta}_r = 0.5$ and four values of γ. These curves can be compared to Fig. 4 to determine the relative effects of $\bar{\delta}_r$. The amplitude responses in Figs. 4 and 8 show the same trends. The rotor with the largest value of $\bar{\delta}_r$ shows the largest amplitudes (Fig. 4). Neither of these cases shows ideal compensation, although the case with $\bar{\delta}_r = 0.5$ has the smallest errors as compared to Fig. 7. The phase angle responses for $\bar{\delta}_r = 0.5$ are somewhat similar to those for $\bar{\delta}_r = 1.0$; namely, the shapes of the phase responses are almost ideal for ω/ω_{cr} greater than 0.7. For $\bar{\delta}_r = 0.5$ and for ω/ω_{cr} less than 0.7, however, the shape of the phase responses for $\gamma = 135$ and 180 deg are significantly different from those for $\bar{\delta}_r = 1.0$. Figure 8 indicates that the slopes of the phase curves are approximately equal to the ideal case at the critical speed. Thus, by using compensation, one can once again accurately determine the system damping by equation (15).

To summarize this last point, Fig. 9 is presented. In this figure, the ratio, ζ/ζ_m, is presented as a function of γ for $\bar{\delta}_o = 0$ and for two values of $\bar{\delta}_r$ and ζ. Two curves are presented in each part of the figure. The first is for a bowed rotor without compensation, while the second is for a bowed rotor with compensation. In most cases, the compensated responses yield accurate values of ζ_m, i.e., $\zeta/\zeta_m \simeq 1.0$. Uncompensated responses often yield significantly high values of ζ_m, particularly for large values of γ. In some cases, the compensated results are in error. For example, in Fig. 9(a) ($\zeta = 0.1$, $\bar{\delta}_r = 1.0$), the value of ζ_m for $\gamma = 169$ deg is found to be infinite since $d\phi/d\omega$ is zero as discussed earlier. Significant errors are only observed for a narrow range of γ in Fig. 9(a). For larger values of ζ, the range of errors in γ for compensated responses increases. For example, in Fig. 9(b) ($\zeta = 1.0$), the range of γ for which errors in measured damping are 50 percent or more is from 0 to 130 deg. For such large values of damping, however, one does not in general need an accurate value in practice, since such machines are rarely encountered and if they are, they are well behaved. For values of $\bar{\delta}_r = 0.5$ (Fig. 9(c)) and 2.0 (not presented), the measured value of ζ (for $\zeta = 0.1$) from the compensated response is very accurate (within 4 percent for all values of γ). For these latter cases, one can examine equation (11) and see that for large values of $\bar{\delta}_r$, the term $\alpha_{rc}\,\bar{\delta}_r$ dominates, while for small values of $\bar{\delta}_r$, the term α_m dominates. Thus, for either large ($\bar{\delta}_r \gtrsim 1.5$) or small bows ($\bar{\delta}_r \lesssim 0.7$), the compensated response appears to be due to strictly a mass unbalance for large values of f ($f \gtrsim 1$). The shape of the phase angle response curve is thus accurate for these cases.

In all of the foregoing discussions and figures, the rotor was assumed to either have bow and no electrical/mechanical runout or vice versa. Several cases of combined bow and runout were also examined but are not presented for the sake of brevity. They did not, however, reveal any different characteristics from those exhibited in Figs. 2-9. One should realize that for a system with a combination of bow and runout, when compensation is used, the runout portion is compensated for correctly, and the bow portion is compensated for incorrectly as predicted earlier. For example, consider a rotor with $\zeta = 0.1$ which has a slow roll ($f \simeq 0$) indicated nondimensionalized vibration amplitude of 2.00 at 90 deg, of which runout is 1.00 at 90 deg and bow is 1.00 at 90 deg. If compensation equal to the slow roll vibration is used, the observed response will be as in Fig. 4, $\gamma = 90$ deg. Namely, the responses are considerably different than the ideal case (Fig. 7) and the differences are predicted by equation (13). Also, the compensated response is much different than the response of a bowed rotor with no compensation and no runout (Fig. 2), particularly the phase.

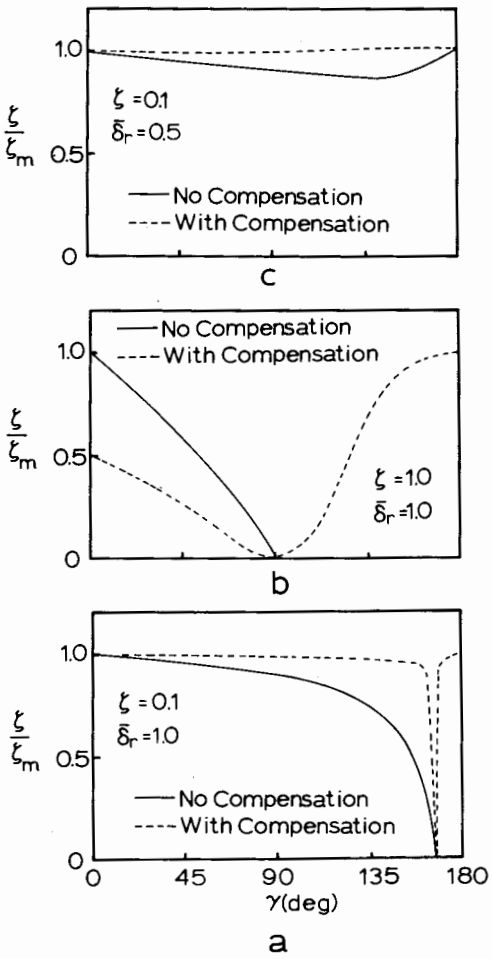

Fig. 9 Ratio of actual and "measured" values of ζ; (a) $\zeta = 0.1$ and $\bar{\delta}_r = 1.0$, (b) $\zeta = 1.0$ and $\bar{\delta}_r = 1.0$, (c) $\zeta = 0.1$ and $\bar{\delta}_r = 0.5$

Only a few typical cases are presented herein. These indicate the particular differences for shafts with bow or runout. Errors in using a runout subtractor for a rotor with bow also have been demonstrated for these cases. Equations were derived in the previous section whereby errors can be predicted for any other conditions not studied herein.

Experimental Apparatus and Procedure

To demonstrate the accuracy of the theoretical results in reference [5] and in this paper, the following experimental analysis was completed. The experimental rig and instrumentation are shown in Fig. 10. The test rotor consisted of a single mass (0.86 kg) centrally located on a 9.53 mm dia steel shaft. The bearing span was 39.05 cm. The rotational speed was controlled with a 1/6 hp dc motor. The first critical speed of the rotor was 2700 rpm.

The rig was instrumented with three displacement transducers. Two were located near the mass and the third was

placed over a notch on one end of the shaft. The two central probes were calibrated and particular probes were chosen such that the two calibration curves were matched. Thus, direct comparison of the outputs of the X and Y probes was possible.

Data were analyzed using a synchronous tracking filter. The notch on the shaft was used as the trigger for the tracking filter. Outputs from the tracking filter included total or synchronous amplitude and synchronous phase angle (measured with respect to the notch). Only synchronous responses are presented in this paper. Reduced data were plotted using an analog plotter. Raw signals from the displacement probes were recorded on an FM tape recorder so that permanent records were obtained for all tests.

The rig was run for very low acceleration rates (less than 50 rpm/s) such that acceleration was negligible [15]. The rig was initially run for the no-bow (ideal) case. From this base run, system damping was determined. The rotor was next run for 12 bowed cases, of which four typical cases are presented herein. Both the amplitude of the bow and its angular position were varied.

Results from the baseline run are presented in Fig. 11. For this initial case, the bow was less than 0.004 mm, as measured by the displacement probes, thus closely representing an ideal unbowed shaft. Dial gages at the center of the shaft also indicated that less than 0.004 mm of mechanical runout was present. Both Bode and Nyquist responses are shown in Fig. 11. These curves were obtained without the use of the compensator in Fig. 10. At 9000 rpm, the response of the rotor was 0.042 mm, while the response at the critical speed was 0.762 mm. Thus, an amplification factor of 18.2 was observed which yields a system damping ($\zeta = 1/2A_{cr}$) of 0.027. Also, by measuring the slope of the synchronous phase angle, one can use equation (15) to determine ζ. This method yielded $\zeta = 0.029$. An average of the two was used ($\zeta = 0.028$) for comparison to theoretical predictions.

After the data for the baseline case were analyzed, bowed rotor cases were run. Shaft warp was induced by loading the shaft at the center until it plastically deformed. The bow was determined by rotating the rotor at slow roll (approximately 400 rpm) and measuring the synchronous response. The mass unbalance was held constant at 0.042 mm and was located in line with the timing mark ($\phi_m = 0$ deg) for all of the bowed rotor runs. The five cases that are presented herein, including the baseline run, are summarized in Table 2. The phase angle of the bow (γ) is measured with respect to the mass unbalance determined from Fig. 11. The cases which were of interest were for $\bar{\delta}_r = 0.5$, 1.0, and 2.0 and $\gamma = 0$, 90, and 180 deg. However, due to the technique of bowing the shaft, the exact bows desired were not obtained. The measured bows are used in the theoretical predictions. In addition, the bow was measured both before and after a test in all cases and did not change by more than 0.004 mm for $\bar{\delta}_r < 1.5$. However, for cases involving particularly large values of $\bar{\delta}_r$ (i.e., approximately 2) the bow changed during the tests by as much as 0.015 mm. In these cases, the bowed shaft could not be simply

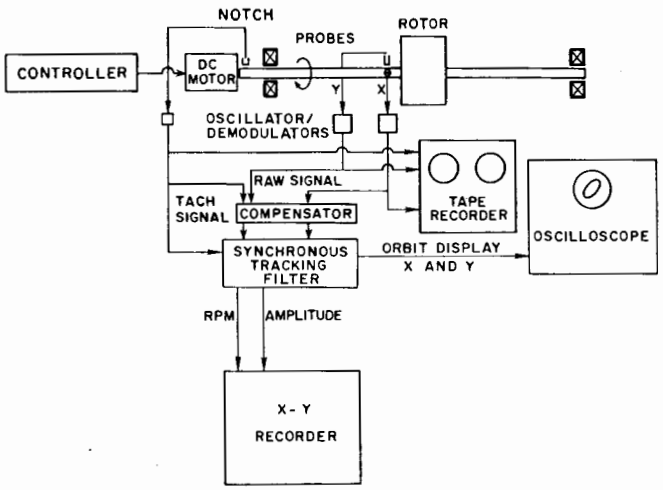

Fig. 10 Instrumentation used

Table 2 Experimental bowed rotor cases

Bow amplitude $\bar{\delta}_r$	Bow phase angle γ (deg)
0.00	0 (Baseline run)
0.36	0
0.90	98
0.66	180
0.99	192

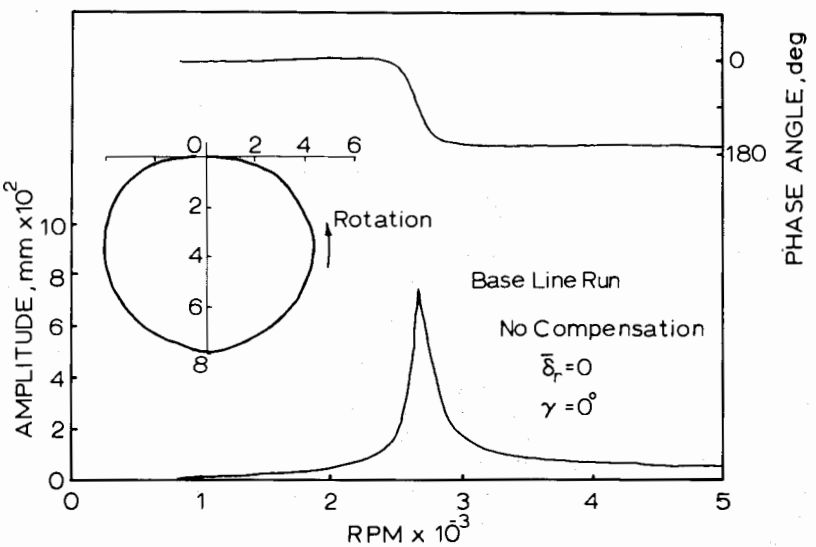

Fig. 11 Base line response ($\bar{\delta}_r = 0, \gamma = 0$ deg)

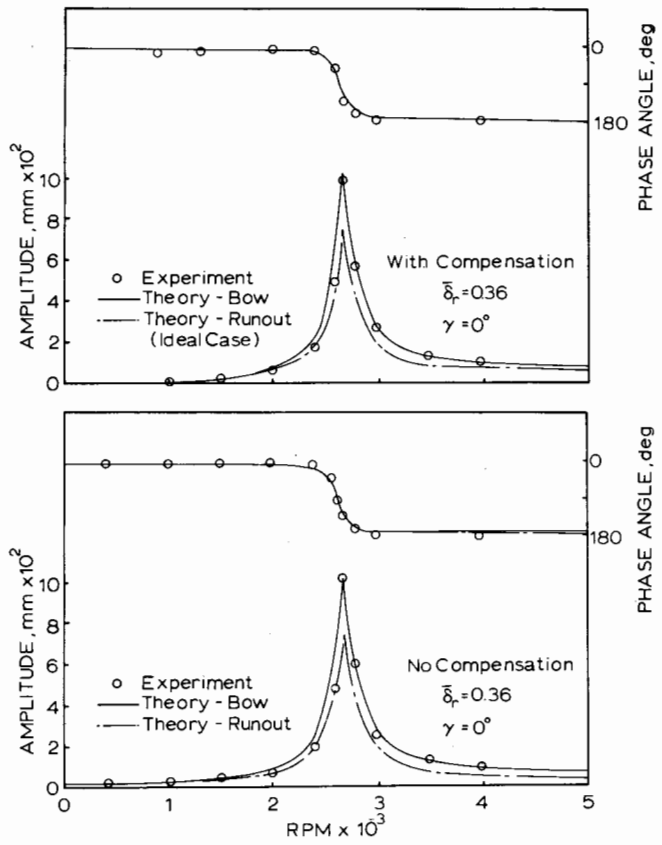

Fig. 12 Response curves for $\bar{\delta}_r = 0.36$ and $\gamma = 0$ deg

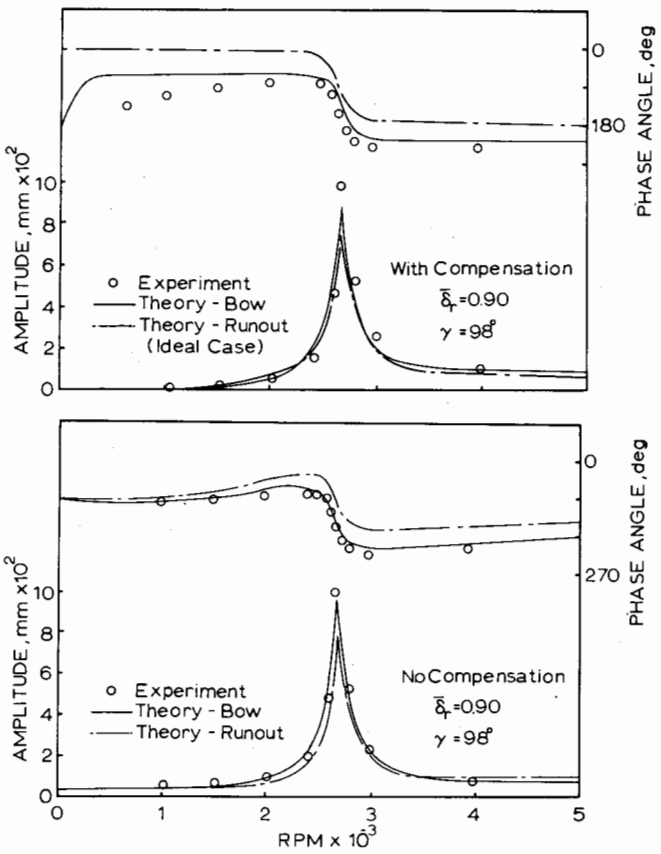

Fig. 13 Response curves for $\bar{\delta}_r = 0.90$ and $\gamma = 98$ deg

modeled and the results of these tests were not considered to be dependable.

The taped vibration data were processed for the cases for a bowed rotor by two methods.

(*a*) The synchronous component of rotor response was plotted as a function of angular speed, ω, using a synchronous tracking filter. The compensator in Fig. 10 was bypassed for these tests.

(*b*) The low speed response (due to bow) was subtracted from the synchronous component of vibrations using the runout compensator plotted as a function of ω. The low speed response was measured at approximately 400 rpm. At this low speed, dynamic shaft forces are small and may be neglected.

Experimental Results

Four typical cases are shown in Figs. 12-15. In these figures, reduced data are presented both without and with low speed compensation. Two sets of theoretical results are also presented on these figures. First, theoretical results using the measured value of $\bar{\delta}_r$ and γ are presented for a bowed rotor. Second, using the measured value of $\bar{\delta}_r$ for $\bar{\delta}_o$ and the measured value of γ for ϕ_o, the theoretical results for a rotor with runout are plotted. Thus, the two theoretical cases display equal low speed responses.

The first case ($\bar{\delta}_r = 0.36$, $\gamma = 0$ deg) is presented in Fig. 12. First consider the uncompensated run. By comparison of the experimental amplitude response to the unbowed case (Fig. 11), one can see that the response at the critical speed is increased due to the bow. For example, the response with no bow is 0.075 mm compared to 0.100 mm with the bow. Also, the theoretical predictions for the model with residual bow is nearly identical to the experimental data, while the model with runout predicts a low value of amplitude at the critical speed. The experimental phase angle response closely resembles that of the unbowed case and also agrees well with the two theoretical predictions, which are nearly identical.

In Fig. 12, the compensated experimental data and theoretical predictions are also plotted. As can be seen, compensation does not greatly affect the results for this case. Theoretical and experimental results for a bowed rotor are in excellent agreement, particularly at the critical speed (less than 3 percent difference in amplitude). The amplitudes of the compensated experimental and theoretical bowed rotor do not, however, agree well with the predicted compensated rotor with runout (ideal) response (27 percent difference at the critical speed).

In Fig. 13, results are presented for $\bar{\delta}_r = 0$ and $\gamma = 98$ deg. The uncompensated amplitude of response is larger than the ideal case (Fig. 11) and is in agreement with bowed rotor predictions. The uncompensated experimental phase angle is seen to increase with increasing speed before decreasing as predicted by bow theory. With compensation, the experimental and theoretical (bow) are again in excellent agreement for rotational speeds greater than 1000 rpm. For lower speeds, the synchronous tracking filter was not able to track phase due to the low amplitude. Also, for speeds greater than 1000 rpm, the shapes of the compensated bow experimental and theoretical phase angle results are in good agreement with theoretical compensated runout results (ideal case), i.e., the slopes are nearly identical.

The case for $\gamma = 180$ deg and $\bar{\delta}_r = 0.66$ is presented in Fig. 14. Also shown in Fig. 14 is the experimental Nyquist form of the response plot. Figure 14 displays several interesting features. (*a*) The experimental uncompensated amplitude becomes zero at 2150 rpm. Bowed rotor theory predicts the amplitude to be zero at 2190 rpm. (*b*) The maximum rotor

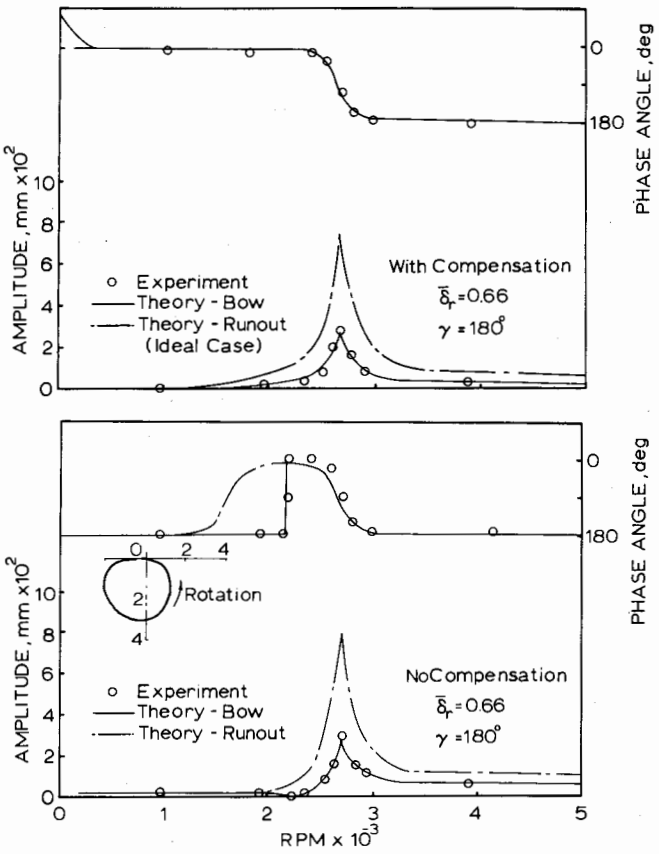

Fig. 14 Response curves for $\bar{\delta}_r$ = 0.66 amd γ = 180 deg

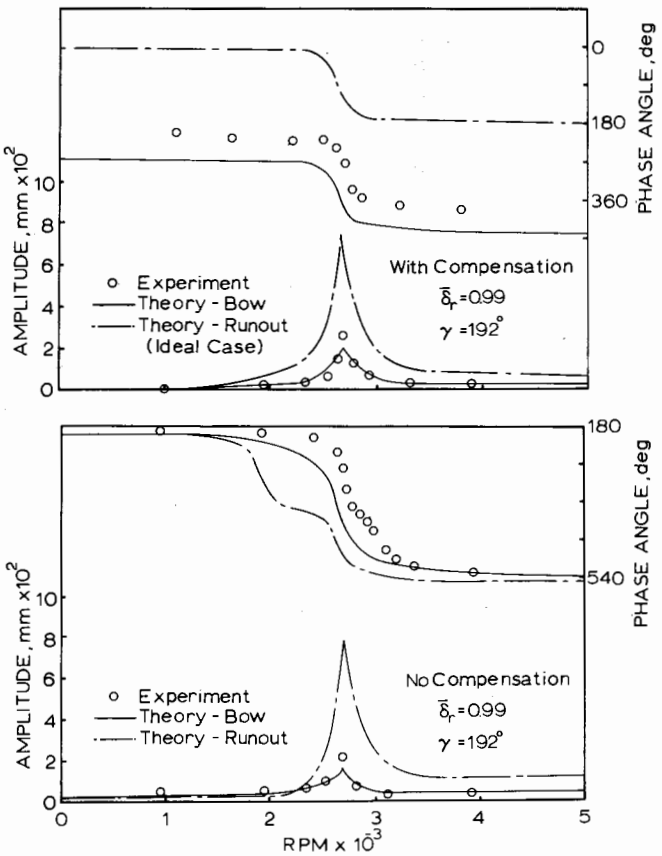

Fig. 15 Response curves for $\bar{\delta}_r$ = 0.99 and γ = 192 deg

response is only 0.29 mm, which is very close to the predicted value of 0.27 mm, but which is significantly different (by over 150 percent) from the amplitude predicted by runout theory (0.76 mm). (*c*) A nearly instantaneous 180 deg phase shift was experienced experimentally at 2150 rpm. This sudden phase shift was predicted to occur at 2190 rpm by bow theory. For comparison, runout theory predicted a gradual shift spanning 500 rpm. This sudden 180 deg phase angle shift represents the time at which the Nyquist response passes through the origin. Also, the radius of the Nyquist plot is significantly smaller than the radius for the unbowed rotor (Fig. 11), as a result of the bow at 180 deg. This observation is consistent with the theoretical predictions earlier in this paper. No "minor" or inside loops are observed on this Nyquist plot. None were observed on any of the other cases run, indicating that bow alone cannot cause such behavior.

In Fig. 14, compensation has small effects on the amplitude response. It does, however, cause the phase angle response to closely resemble the ideal response for speeds greater than 1000 rpm.

The final case is presented in Fig. 15 and has $\bar{\delta}_r$ = 0.99 and γ = 192 deg. In Fig. 15, the maximum experimental amplitude is only 0.21 which agrees with bowed rotor theory well but is not in agreement with runout theory (0.75 mm). The experimental phase angle also agrees well with bow theory. A net phase angle shift of 360 deg is experienced which agrees with the observations of a large scale test rig [14]. When $\bar{\delta}_r \simeq$ 1.00 and γ is slightly larger than 180 deg, a 360 deg phase shift is seen. The phase angle response for a rotor with runout is also seen to shift by 360 deg. This runout curve has a "plateau" at 380 deg as compared to the bowed rotor prediction which is smooth. The experimental data do have a very slight plateau which indicates a small amount of runout is present.

The compensated results for the final case are also presented in Fig. 15. The experimental results again compare well with the bowed rotor predicted results. The shapes of the three phase angle curves are very similar for speeds in excess of 1000 rpm.

Conclusions

A Jeffcott rotor was theoretically modeled having both a bowed shaft and electrical/mechanical runout. A theoretical model was also developed to employ constant subtraction of the slow roll amplitude of vibration from the response amplitude. Equations were derived whereby the response and compensated response for any bow, unbalance, and runout can be calculated. Equations are also presented whereby the errors associated with runout subtraction applied to a bowed rotor can be estimated. Samples cases were presented demonstrating the use of the equations.

A small rotor was also experimentally tested with various values of bow. The rotor was first tested with no bow and then tested with 12 vectoral values of bow, of which four are presented herein. The data were analyzed both not using and using low speed (slow roll) compensation. Experimental results are compared to theoretical predictions for both bowed rotors and rotors with runout.

Specific conclusions include the following.

1 Significant differences in theoretical response plots for rotors with runout and bow are evidenced. The most pronounced differences are observed in Nyquist plots where the relative response of a bowed rotor is strongly dependent on the circumferential position of the bow, i.e., the radius of the Nyquist circle varies with γ. The relative responses of a rotor in a Nyquist plot with runout are not a function of

circumferential location, i.e., the radius of the Nyquist circle does not vary with ϕ_o.

2 When the phase angle of the bow is equal to 180 deg, a sudden phase angle shift of 180 deg is theoretically predicted at a value of ω/ω_{cr} dependent on $\bar{\delta}_r$. However, no such sudden shift in phase angle is present with a rotor with runout.

3 For a bowed rotor with $\bar{\delta}_r = 1.00$, a particular phase angle is predicted (which depends on ζ) for which the response is nearly constant for all rotational speeds. For $\zeta = 0.1$, this angle is predicted to be approximately 169 deg.

4 Employing compensation to a rotor runout not incur any errors as should be expected. Employing such compensation for bowed rotors has been predicted to incur significant errors. The amplitude response plots are not improved with compensation. The shapes of the phase angle responses are incorrect for low values of ω/ω_{cr} but closely approximate the ideal phase angle plots for $\omega/\omega_{cr} \gtrsim 0.7$.

5 By measuring the slope of the phase angle in a Bode plot at the critical speed, one can determine the system damping for an unbowed rotor without runout. Such a technique for a bowed rotor without compensation usually leads to significant errors. However, by using such compensation the errors are predicted to be reduced to 5 percent or less.

6 For cases with combined bow and runout, if a compensator is used the indicated response is the bowed rotor response with compensation.

7 Experimental results compare much better to bowed rotor predictions than to predictions for a rotor with runout.

8 Low speed compensation does not cause the amplitude response to represent the ideal unbowed rotor response, as shown experimentally.

9 Low speed compensation does cause the shape of the phase response to closely represent the ideal unbowed rotor response, as shown experimentally.

10 The radius of the response in Nyquist form is strongly dependent on the bow vector, as shown experimentally.

Acknowledgments

This research was sponsored by the Industrial Supported Program for the Dynamic Analysis of Turbomachinery at the University of Virginia, directed by Dr. E. J. Gunter, and by the Department of Energy under contract DE-AC01-79ET-13151, under the direction of Dr. D. W. Lewis. The authors also acknowledge the helpful discussions with Dr. P. E. Allaire and Mr. J. D. Heinzmann.

References

1 Lewis, D. W., Flack, R. D., and Gunter, E. J., "Instrumentation and Experimental Findings With a Flexible Rotor System," *Proceedings of the 1979 Symposium Instrumentation and Control for Fossil Energy Processes*, Aug. 20-22, 1979, pp. 360-375.

2 Jackson, C., *The Practical Vibration Primer*, Gulf Publishing Co., 1979.

3 Jackson, C., "Using the Orbit to Balance," *Mechanical Engineering*, Vol. 93, No. 2, Feb. 1971, pp. 28-32.

4 Thompson, W. T., *Theory of Vibration with Applications*, Prentice-Hall, New Jersey, 1972.

5 Nicholas, J. C., Gunter, E. J., and Allaire, P. E., "Effect of Residual Shaft Bow on Unbalance Response and Balancing of a Single Mass Flexible Rotor, Part 1: Unbalance Response," ASME *Journal of Engineering for Power*, Vol. 98, No. 2, Apr. 1976, pp. 171-181.

6 Newkirk, B. L., "Shaft Rubbing," *Mechanical Engineering*, Vol. 48, 1926, p. 830.

7 Dimarogonas, A. D., "An Analytical Study of the Packing Rub Effect in Rotating Machinery," Ph.D. dissertation, Rensselaer Polytechnic Institute, Troy, New York, 1970.

8 Kikuchi, K., "Analysis of Unbalance Vibration of Rotating Shaft System with Many Bearings and Disks," *Bull. J.S.M.E.*, Vol. 13, No. 61, 1970, pp. 864-872.

9 Yamamoto, T., "On the Critical Speeds of a Shaft," Memoirs of the Faculty of Engineering, Nagoya University, Japan, Nov. 1954.

10 Parkinson, A. G., Jackson, K. L., and Bishop, R. E. D., "Some Experiments on the Balancing of Small Flexible Rotors: Part II—Experiments," *Journal of the Mechanical Engineering Science*, Vol. 5, No. 2, 1963, pp. 133-145.

11 Nicholas, J. C., Gunter, E. J., and Allaire, P. E., "Effect of Residual Shaft Bow on Unbalance Response and Balancing of a Single Mass Flexible Rotor, Part II: Balancing," ASME *Journal of Engineering for Power*, Vol. 98, No. 2, Apr. 1976, pp. 182-189.

12 Salamone, D. J., and Gunter, E. J., "Effects of Shaft Warp and Disk Skew on the Synchronous Response of a Multimass Rotor in Fluid Film Bearings," *Topics in Fluid Film Bearing Design and Optimization*, ASME, 1978, pp. 79-107.

13 Flack, R. D., Leader, M. E., and Gunter, E. J., "An Experimental Investigation on the Response of a Flexible Rotor Mounted in Pressure Dam Bearings," ASME JOURNAL OF MECHANICAL DESIGN, Vol. 102, No. 4, Oct. 1980, pp. 842-850.

14 Leader, M. E., Flack, R. D., and Lewis, D. W., "An Experimental Determination of the Instability of a Flexible Rotor in Four Lobe Bearings," *Wear*, Vol. 58, No. 1, Jan. 1980, pp. 35-47.

15 Hassenpflug, H. L., Flack, R. D., and Gunter, E. J., "Influence of Acceleration on the Critical Speed of a Jeffcott Rotor," ASME *Journal of Engineering for Power*, Vol. 103, No. 1, Jan. 1981, pp. 108-113.

Printed in U.S.A.